A Detailed Postprocess Analysis of an Argon Gas Puff Z-pinch Plasma Using SPEC2D

Y. K. Chong, T. Kammash and J. Davis*

Dept. of Nuclear Engineering, University of Michigan, Ann Arbor, MI 48109
**Radiation Hydrodynamics Branch, Naval Research Laboratory, Washington, DC 20375*

Abstract. A postprocess analysis of a single time frame hydrodynamic profile from the PRISM two-dimensional MHD simulation of an argon gas puff Z-pinch plasma experiment on Double-Eagle generator at Physics Internationals, Co. is presented. In addition, spatially resolved emission spectra and filtered (K- and L-shell radiation) x-ray pinhole images, generated using the SPEC2D code, are examined toward the understanding of the emission characteristics of the hot spots and the formation of the Rayleigh-Taylor instability in the plasma.

I Introduction

The PRISM two-dimensional MHD code has been used to simulate a series of argon gas puff Z-pinch plasma experiments on the 4 MA, 6 TW Double-Eagle facility at the Physics International, Co. in order to predict and understand the effects of nozzle tilting on the stability and uniformity of the plasma as a high energy plasma radiation source [1]. In this paper, we apply the two-dimensional non-LTE radiation ID code, AXSTRAN [2], as a postprocessor toward a detailed understanding of the radiation and ionization physics in the plasma. We focus the analysis on a single time frame hydrodynamic profile from the PRISM simulation of an argon Z-pinch plasma generated from an annular 2.5 cm diameter Mach 4 nozzle with an exit width 0.5 cm that is tilted inward at 10 degree to minimize the "zippering." In addition, synthetically generated spatially resolved emission spectra and filtered (K- and L-shell) pinhole images are examined for the understanding of the radiation characteristics of the hot spots and the formation of the Rayleigh-Taylor instability in the plasma.

II SPEC2D

In order to generate both spatially and spectrally resolved emission spectra and images of an axisymmetric 2-D plasma, a spectrum image synthesis code, SPEC2D, was developed. The code is based on the multifrequency integral transport method wherein the intensity at each spectral value is determined from numerical integration of the formal solution of the radiative transfer equation along the line-of-sight rays propagating through the plasma and then incident on an experimental device. The code allows for any arbitrary observation position and viewing angle of the device, and accommodates the variation in the observables from a narrow band spectrometer to a broad-angle imaging camera. Schematic representation of an experimental setup that served as the model for the SPEC2D is depicted in Fig. 1 which shows a pinhole camera, located at the distance L_d from the plasma axis and Z_d from the plasma midplane and with the viewing angle θ_d relative to the center of the plasma. Once, a family of rays are defined by projecting a line of sight ray from each discretized pixel position (r_c, z_c) on the camera film toward and passing through the plasma region of interest, the measured specific intensity associated with each ray (with an appropriate solid angle factor, ω_c, weighted for the pixel area) may

CP409, *Dense Z-Pinches*: Fourth International Conference
edited by N. R. Pereira, J. Davis, and P. E. Pulsifer

be expressed as

$$I_\nu^m(r_c,z_c,L_d,Z_d,\theta_d)=\omega_c\int_0^\infty d\nu' R(\nu,\nu')\int_0^{|\underline{x}_o-\underline{x}_i|} ds' j_\nu(\underline{x}_o-s'\underline{\Omega})e^{-\int_0^{s'}\kappa_\nu(\underline{x}_o-s''\underline{\Omega})ds''}, \quad (1)$$

where R is the spectral response function of the film, $\underline{\Omega}$ is the direction of the ray and $\underline{x}_i$ ($\underline{x}_o$) is the plasma entrance (exit) point of the ray. The emissivity, j_ν, and opacity, κ_ν, profiles are deduced from the self-consistently determined radiation field, ionization states and temperature and density of the plasma using the AXSTRAN code. Numerical integration of Eq. (1) through the three-dimensional space occupied by the plasma is obtained exactly using the ray-based radiation transport technique of AXSTRAN.

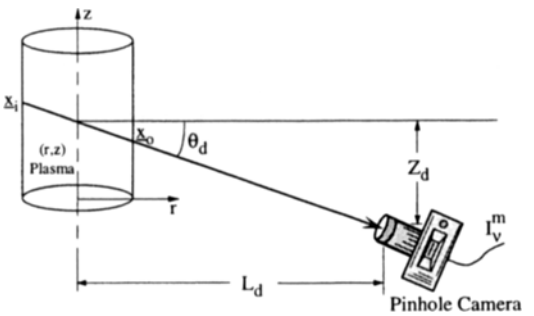

Fig. 1 Schematic representation of an experimental setup serving as the model for the development of SPEC2D.

III Results

The mass and internal energy density profiles of the argon plasma generated by the PRISM code near peak compression time (t = 100 nsec) are analyzed using the AXSTRAN code. The plasma is characterized by the initial dimensions of 3 cm in length and radius 1.25 cm, and a linear mass density of 50 $\mu g/cm$. CRE is assumed for the plasma, and the details of the argon atomic model used as well as the transport calculation can be found in Ref. 2.

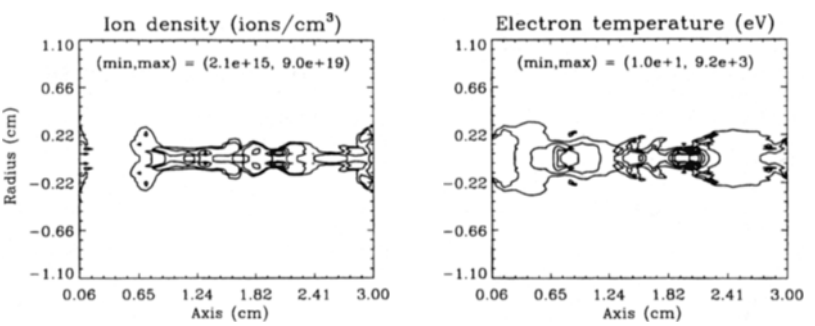

Fig. 2 Temperature and density profiles of the argon plasma at t=100 nsec.

The calculated ion density and electron temperature profiles are presented in Fig. 2 and show that the bulk of the plasma has stagnated near the axis with the typical radius of about 2 mm and the peak ion density of $9x10^{19}$ ions/cm^3. It is, however, highly nonuniform and may be m=0 unstable. The stagnant plasma has a temperature (over 1 keV) which is sufficient for the emission of high energy K-shell radiation. The plasma at this temperature and density regime should be somewhat optically thick to the bound-bound (b-b) lines and quite thin to the continuum radiation.

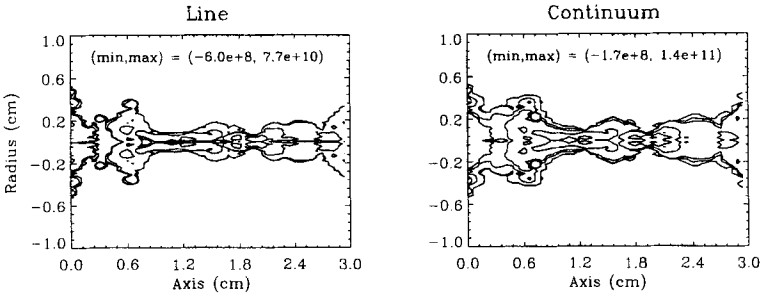

Fig. 3 Line and continuum radiative power densities in units of kW/cm^3.

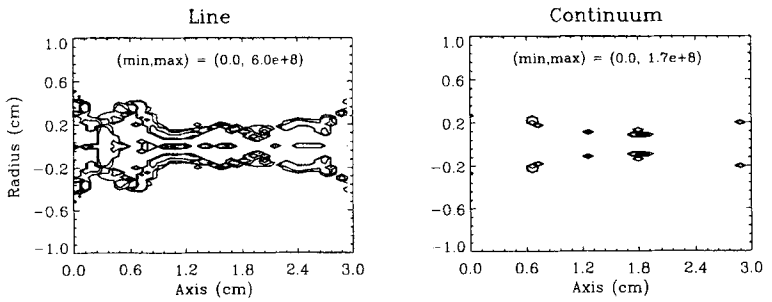

Fig. 4 Line and continuum radiative heating rates in units of kW/cm^3.

The contour plots of the line and continuum radiative power densities in the plasma are presented in Fig. 3 and show that the b-b emission is more significant near the axis and narrower than the continuum emission. This is due to the fact that the core of the plasma is hotter and denser than the outer plasma regions. The total b-b and continuum powers are 0.32 and 0.29 GW, respectively, which are compared to 1.1 and 0.28 GW in the optically thin case. This validates an earlier assertion that the lines are moderately thick while the continuum is thin. The K (L) -shell radiation represents 70 (30)% of the total power, indicative of the relatively high temperature of the bulk plasma. As the high flux of the radiation from the hot and dense core region propagates outward toward the cooler outer region, it provides an efficient means by which the inner plasma cools and transfers the energy to and heats the outer plasma. This is illustrated in Fig. 4 which shows the net radiative absorption or heating rate for the lines and continuum. We notice that the most significant radiative heating occurs at the outer region immediately surrounding the core plasma. The heating is dominated by the b-b processes which represents 97.6% of the total radiation absorbed whereas the continuum constitutes 0.66% and the inner-shell absorption is a non-insignificant fraction with 1.8 % of the total. In this respect, the radiation acts as an energy redistribution agent toward smoothing out of the gradients in the temperature, and hence, in the ionization states as will be seen below.

The effects of the radiation transport on the atomic level distribution are illustrated in Fig. 5 which shows the optically thin and thick fractional population densities for the C-like Ar XVIII ion. When the radiation is ignored, the ion is nonnegligible only at few small spots just beyond the bulk plasma. Once the absorption of the hot core photons is taken into account, however, the photopumping effect on the ion population is immediate and quite drastic. The figure shows that all surrounding outer regions are lit up and highly photo-enhanced by the core photons. The spatial distribution of the resulting ion population is strongly nonuniform due to the gradients and nonuniformities in the plasma temperature and density as well as in the radiation field. The net effect is that the radiation has driven the plasma to a significantly higher ionization state (the effective charge of the outer burnedup region increased on the average by a factor of 2 or more from the local thin value). In general, the radiation effect on the plasma ionization state should lessens as a function of radius because, as the photons from the inner core get absorbed and ionize the plasma, their probability of reaching a larger radius diminishes. This is illustrated in Fig. 6 which presents the radially resolved population density ratio (thick over thin) plots for selected argon ground states at z = 2.1 cm. Note the variation in the ratio as a function of radius and for different ion states.

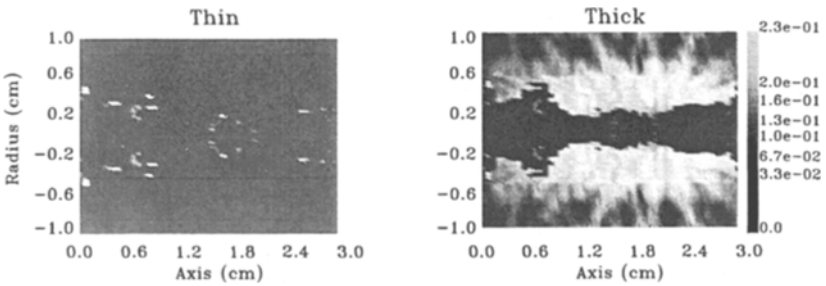

Fig. 5 Optically thin and thick fractional population density plots for the C-like Ar XIII ion.

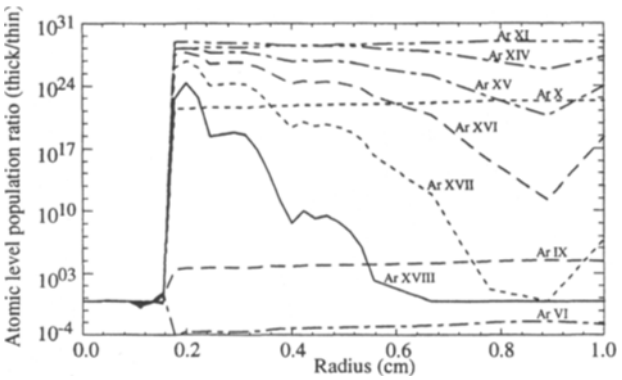

Fig. 6 Radially resolved population density ratio (thick/thin) curves for selected Ar ground states at z = 2.1 cm.

Synthetic K- and L-shell x-ray pinhole images of the plasma taken from a camera located at (L_d, Z_d) of (100, 1.5) cm and oriented toward the plasma center are presented

Fig. 7. The images show that both the K- and L-shell emissions are dominated by a small number of hot spots on the order of 1 mm radius and of varying axial lengths from 1 to 3 mm located along the axis. In particular, the hottest and densest hot spot, located at z = 2.1 cm with rough physical dimensions of radius 0.5 mm and 2 mm in length, has the peak radiative power of 217 GW/cm^3 or the emission rate of 0.34 GW. This represents 55.7% of the total radiative power (0.61 GW) in the plasma, and hence a major fraction of the total radiative cooling rate. We also observe that the L-shell emission image is broader than the K-shell image. This is expected since the plasma temperature and density increase sharply near the core while they become broader and lower away from the core. Both the K- and L-shell images exhibit a strong spatial intensity variation, indicative of the underlying structures and inhomogenieties (most likely from the formation of the

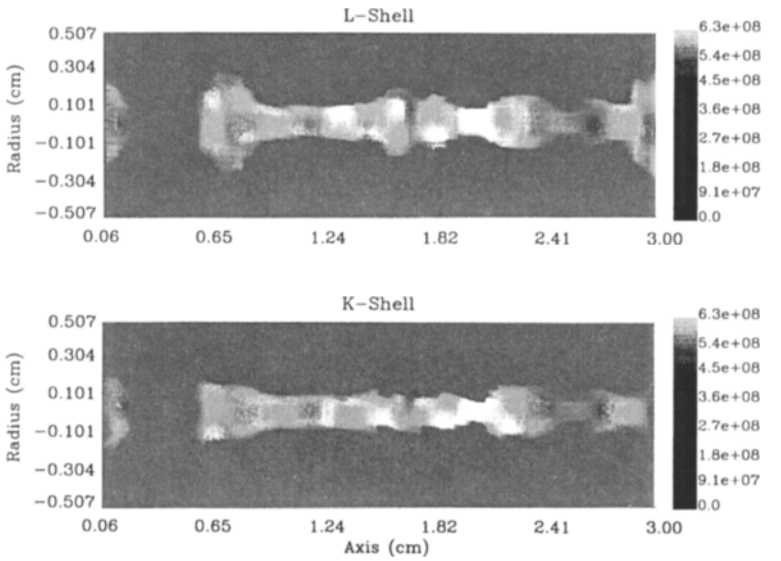

Fig. 7 Synthetic filtered (K- and L-shell radiation) pinhole images of the plasma taken from (L_d, Z_d) of (100, 1.5) cm and viewed along the plasma center.

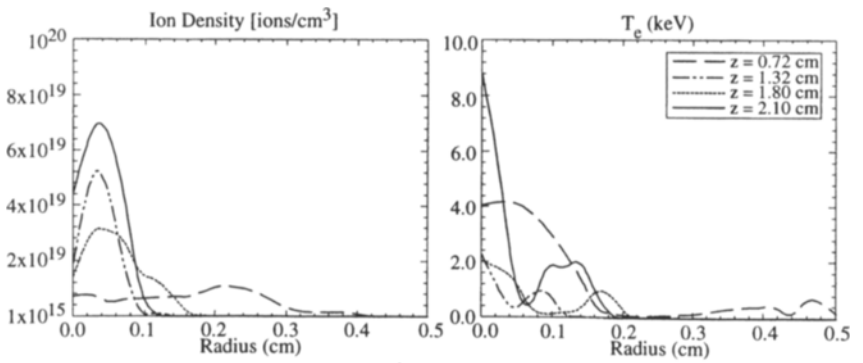

Fig. 8 Radially resolved ion density and temperature for selected hot spots.

Rayleigh-Taylor and/or m=0 instabilities). Unfortunately, the deciphering of the internal structures from the analysis of the images alone would be a difficult task since the images represent spatially averaged quantities along the line of sight rays. In this regard, the radially (and/or axially) resolved temperature and density profiles, as shown in Fig. 8 for selected hot spots, can be useful toward the understanding of their emission characteristics as a function of temperature, density and size. For example, the hot spots at z = 1.32 and 1.80 cm are warm and dense with a hollow core and thus manifest themselves with the corresponding L-shell image being brighter than the K-shell image and with the radial intensity variations which reflect the underlying temperature and density gradients. Finally, the lateral emission spectra across the selected hot spots are presented in Fig. 9. It shows a wide and significant divergence in the number and intensity of spectral features, reflective of different radial variations in the temperature and density profiles and size of the hot spots and the plasma surrounding them.

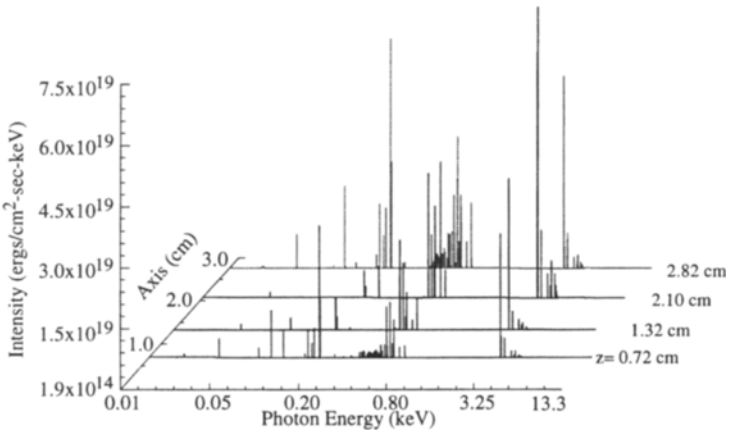

Fig. 9 Calculated lateral emission spectra across selected hot spots.

IV Conclusion

A detailed postprocess analysis of the radiation and ionization physics of an argon gas puff Z-pinch plasma was carried out. It was shown that the radiation and its nonlocal energy transport significantly affects the plasma physics and energetics and whose property is highly influenced by the temperature and density gradients and nonuniform structures in the plasma. An analysis of the hot spots from the synthetic K- and L-shell x-pinhole images generated by SPEC2D confirmed the wide variation in their temperature, density and size characteristics and pointed to the underlying inhomogenieties due to the Rayleigh-Taylor and MHD instabilities.

References

1. C. Deeney, P. D. LePell, F. L. Cochran, M. C. Coulter, K. G. Whitney and J. Davis, Phys. Fluids B 5, 992 (1993).

2. Y. K. Chong, T. Kammash and J. Davis, in this proceeding.